Open Access

Journal of Energy and Power Technology

LIDSEN Publishing Inc.

Research Article

The Liquid-Mediated Synthesis and Performance Evaluation of Li-Zr-F Composite for Ion-Conduction

Junmo Moon [1], Satita Thiangtham [1], Ruijie Zheng [1], Sicheng Liu [1], Chayanaphat Chokradjaroen [1], Yasuyuki Sawada [1, 2, 3], Nagahiro Saito [1, 2, 3, 4, *]

1. Department of Chemical Systems Engineering, Graduate School of Engineering, Nagoya University, Furo-cho, Chikusa-ku, Nagoya, 464-8603, Japan; E-Mails: junmo.moon89@gmail.com; aon@sp.material.nagoya-u.ac.jp; zheng.r.ab@m.titech.ac.jp; lius@sp.material.nagoya-u.ac.jp; eig@sp.material.nagoya-u.ac.jp; ysawada@sp.material.nagoya-u.ac.jp; hiro@sp.material.nagoya-u.ac.jp
2. Japan Science and Technology Corporation, Open Innovation Platform with Enterprises, Research Institute and Academia, Furo-cho, Chikusa-ku, Nagoya, 464-8603, Japan
3. Japan Science and Technology Corporation (JST), Strategic International Collaborative Research Program (SICORP), Furo-cho, Chikusa-ku, Nagoya, 464-8603, Japan
4. Conjoint Research Laboratory in Nagoya University, Shinshu University, Furo-cho, Chikusa-ku, Nagoya, 464-8603, Japan

* **Correspondence:** Nagahiro Saito; E-Mail: hiro@sp.material.nagoya-u.ac.jp

Academic Editor: Osamu Yamamoto

Special Issue: Battery Materials for Energy Conversion

Journal of Energy and Power Technology
2023, volume 5, issue 1
doi:10.21926/jept.2301010

Received: December 04, 2022
Accepted: February 12, 2023
Published: February 20, 2023

Abstract

Crystalline lithium fluoride (LiF) has been intensively pursued as potential alternative solid electrolytes (SEs) owing to its excellent chemical and electrochemical oxidation stability, and good deformability. However, due to its low ion conductivity, LiF is still challenging for practical SE applications. Herein, Li-Zr-F composite-based SE by liquid-mediated synthesis is proposed to be studied. methanol (CH_3OH) was mainly evaluated as a liquid-mediated precursor for synthesizing Li-Zr-F composites under the stoichiometric proportion of LiF and

ZrF4 (2:1 and 2:0.8) and a subsequent annealing process at 25°C/150°C, 50°C/150°C, and 70°C/150°C, respectively. X-ray diffraction results revealed that the Li-Zr-F composites could be crystallized in the three main types of phase formations, including Li_2ZrF_6 ($P21/c$), Li_2ZrF_6 ($P\overline{3}1m$), and Li_4ZrF_8 ($Pnma$) octahedron structures. In addition, the effect of cation Zr^{4+} stack sublattice synthesized by methanol mediator on the ion conduction of Li-Zr-F composites was investigated by using electrochemical impedance spectroscopy (EIS). Through the Zr^{4+}-substitution, Li_2ZrF_6 ($P\overline{3}1m$)-based SE exhibited the highest ion conduction which was increased to 2.40×10^{-8} S/cm and 3.89×10^{-8} S/cm under the stoichiometric proportion of LiF and ZrF_4 2:0.8 at a dried temperature of 50°C/150°C with, respectively. A 0.21 eV activation energy (E_a) was achieved for a battery with Li_2ZrF_6 ($P\overline{3}1m$)-based SE. Meanwhile, LiF exhibited E_a up to 0.78 eV leading to a low kinetic rate for ion diffusion. These results implied that Li_2ZrF_6 ($P\overline{3}1m$)-based SE was successfully synthesized under the optimal condition of CH_3OH-50°C/150°C which could improve the ion-conductivity of LiF.

Keywords
Ion-conduction; LiF solid electrolyte; liquid-mediated synthesis; turning defect

1. Introduction

Regarding environmental concerns and the goal of sustainable development, solid-state batteries (SSBs) are considered a new candidate energy storage technology to be the next generation of batteries. Solid electrolytes (SEs) are essential component that adapt from a lithium metal anode to a cathode [1]. Typically, the SEs are incorporated in the battery, mainly to resolve the electrolyte leakage, flammability, and limited energy density of liquid electrolytes [2]. Compared with conventional liquid batteries, known as lithium-ion batteries, SEs show superior performance, higher safety in electric vehicles (EVs) and operational durability [3, 4]. Nonetheless, the fabrication of the architecture is still challenged by interfacial issues between the electrode and SEs, generally due to the instability of the SEs against the metallic anode and cathode, obstructing their use in practical applications. Owing to the grain boundaries, pores, and even single crystals of SE, which are generated, the irregular electric-field distribution and poor interfacial contact with the electrodes leading to the introduction of the dendritic deposition cause rapid short-circuiting of the battery [5-9]. These side reactions generally occur during repeated charge/discharge, which increases interfacial resistance and greatly inhibits battery performance. Various strategies have been proposed to overcome these limitations of SBBs by developing new types of SE, which can be classified into solid polymer electrolytes (SPEs), inorganic ceramic electrolytes (ICEs), and solid composite electrolytes (SCEs) in order to enhance the interfacial contact stability between SE and electrode [10, 11]. Exceptionally, an attractive feature of ICEs coming onto the stage such as LiPON, oxide-, sulfide-, hydride-, and halide-based SEs, exhibit good mechanical properties, nonflammability, high-temperature stability, and greater ionic conductivity [10]. Due to their high ionic conductivity of over 10^{-3} S cm^{-1} at ambient temperature, the oxide- and sulfide-based SEs are provided to be the candidates for utilization in SSBs [10-12]. Notwithstanding, the rigid oxide-based SE and thermodynamically unstable with high-voltage oxide cathode materials of sulfide-based SEs

might have limited practical use, especially the manufacturing complexity on a large scale and sensitivity to the air [11, 13].

In comparison, halide-based SEs such as F-, Cl-, and Br-, etc., [14] anion compounds with higher electronegative than oxide and sulfide, exhibit the wide thermodynamic range of electrochemical stability windows with electrode materials, which have demonstrated potential application in SSBs. [11, 15] Among halide-based SE materials, crystalline lithium fluoride (LiF) is altering as the new candidate with a wide electrochemical stability window (0-6.4 V vs Li/Li^+) and good chemical stability with electrodes which could aid high energy density of batteries [16, 17]. Unfortunately, due to the strong bonding between Li and F ions in the LiF structure, thus, making it has high stability leading to hampering the diffusivity of the, suffering from the low contribution of ionic conductivity 10^{-13} S/cm at RT [18]. Hence, it would be desirable to design the lattice structure to prevent coupling bonding of Li-F and to trigger a fast diffusion of Li^+ without compromising its intrinsically high electrochemical stability [16, 18]. It was widely acknowledged that the relationship between the ionic conductivity of electrolytes and their crystal orientations was related to the number of vacancies, interstitials, and partial occupancy on interstices or lattice sites [19]. Additionally, a strong correlation between the orientated Li^+ sublattice and the energy barrier of Li^+ migration might also be affected to enhance the ion conduction of LiF-based SEs with low activation energy (E_a) [11, 20]. Thus, based on the concept of cation sublattice and ion arrangement, it could be implied that the structure of Li-M-F, M as the metal-transition cation in high oxidations states (M^{3+}: Co, Ni; M^{4+}: Mn, V, Cr, Ni, M^{5+}: Cr) [21], resulted in the possible structure design to increase its ionic conductivity by the substitution of heterovalent cation to dilate the spatial lattice of crystal layer, known tuning-defect chemistry [19, 22]. Through the vacancies mechanism, the Li^+ hopping process was sensitive to the active Li^+ and vacancy concentration, which might result in order magnitude changes in conductivity. Additionally, based on their electrostatic forces, the stacking structure of LiF by layered cation ionic crystals with distinctive radii could be arranged in crystal orientation [19]. Microstructural effects increased the ion conduction values of LiF through the sub-layered of metal by space-charge effects between Li-M-F causing the enhancement of the degree of amorphization [23]. For example, in 2017, J. Xie et al. [16]. Successfully synthesized $LiAlF_4$-SE thin film via atomic layer deposition (ALD). The $LiAlF_4$-SE thin film exhibited higher performance with robust stability and satisfactory ion conductivity than LiF and AlF_3. The result demonstrated that the wide range of the predicted stable electrochemical window of approximately 2.0-5.7 V vs. Li^+/Li for $LiAlF_4$ led to excellent interfacial stability with both electrodes, causing a higher ion conductivity was evaluated at 3.5×10^{-8} S/cm. Moreover, M. Feinauer et al [24]. Reported that a high-energy ball-milling method could be utilized to synthesize β-Li_3AlF_6. After mechanical milling of LiF and AlF_3 for 20 h at 600 rpm, the crystal structure of β-Li_3AlF_6 was formed. An ionic conductivity of 3.9×10^{-6} S/cm was observed at 100°C. Even though the ion conduction of Li-M-F formation might be improved, most Li-M-F SEs were synthesized with energy-intensive and time-consuming processes, including high-force and energy ball-milling and high-temperature annealing process led to energy waste [10, 12, 25].

To address these issues, the liquid-mediated synthesis routes would be suggested as a promising method to synthesize Li-M-F compounds with much more energy-friendly and time-saving [10, 26]. Recently, Li et al., [12] studied a method to directly synthesize high-performance Li_3InCl_6-based SE in water, with ionic conductivity as high as 2.04×10^{-3} S/cm, under a simple synthesis method. The reactants were dissolved in water, then dried in the air to obtain the Li_3InCl_6 product. Then, in 2020

Hu et al., [27] reported a dissolution-precipitation method based on the ionic liquid to synthesize Li_3GaF_6 fluoride-based SE by combining Li_2CO_3 and $Ga(NO_3)_3{\cdot}xH_2O$, as raw materials, in $C_{10}mimBF_4$ ionic liquid. The ion conduction of Li_3GaF_6 fluoride-based SE had been improved up to 10^{-4} S/cm at RT. However, there are only a few publications to study the effect of aqueous solutions such as water or ethanal media on the synthesis of halide electrolytes, a lack of knowledge that hampers the development of SEs. Herein, the novel synthesis with methanol has been studied for Li-Zr-F-based SE via facile synthesis, energy-friendly conditions and short processing consuming time and post-treatment. The methanol-mediated precursor was mainly composed of methanol-coordinated halides and organic fragments to synthesize LiZrF-based SE. The organics in the precursor would vanish in the form of gas release including H_2, CH_4, H_2O, -OH, methylene oxide (H-CHO), and some unknown ionized fragments generated post-treatment. Moreover, considering the creation of vacancy clusters in the SE, a tetravalent valence cation was proposed to develop the ion conduction of LiF material. Zirconium (Zr), a metallic element of group 4, has the highest valence state of tetravalence and three inherent vacancies which were proposed to introduce the stacking layer of stabilized metal halide structure to form Li-Zr-F (LiZrF) ionic crystals. The different radius atoms were affected by the arrangement of crystal lattice based on their electrostatic forces. Based on the radius atom of Zr^{4+}(0.72 Å), it exhibited the nearest neighbor within Li^+ (0.76 Å) sublattice which could be implied as a good structural descriptor in certain intrinsic Li^+ mobility attributed to vacancy size matching [18, 21]. Through substituting Zr^{4+} cation and under optimal synthesized conditions, Li_2ZrF_6 formation, built by the edge-sharing ZrF_8 polyhedrons, demonstrated the stabilized structure and rigid framework as isolated lagers in the bc-plane. Between the layers of ZrF_8 polyhedrons were occupied by the sandwiched edge-sharing LiF_6 octahedrons. Thus, making each of Li^+ in layered Li_2ZrF_6 might diffuse along a 2D channel in bc-plane, from one octahedral site to another. The electrochemical impedance spectroscopy (EIS) test demonstrated that Li_2ZrF_6-based SEs exhibited superiors ion conduction of 2.40×10^{-8} S/cm and 3.89×10^{-8} S/cm than LiF-based SE (1×10^{-8} S/cm), which were synthesized under the stoichiometric proportion of LiF and ZrF_4 2:0.8 at a dried temperature of 50°C/150°C with, respectively. Exceptionally, via the stoichiometric proportion of LiF and ZrF_4 2:0.8, named Li-Rich LiZrF-based SE, revealed the electronic conductivity of 3.42×10^{-9} S/cm, which was lower than the ionic conduction, approximately 10% of the overall conductivity with the activation energy (E_a) of 0.21 eV. This significant relationship corresponded to the theoretical crystal formation and the preferred orientation that might directly affect the polyhedrons, through which migration might be fast with low activation energies in crystalline conductors.

2. Materials and Methods

2.1 Materials

Lithium fluoride (LiF), high purity grade ≥99.98% trace metals basis (≤100 μm) and Zirconium (IV) fluoride (ZrF_4), high purity grade 99.9% and $LiNi_{0.8}Co_{0.1}Mn_{0.1}O_2$ (NCM811) trace metals basis and carbon black were supplied from Sigma Aldrich. Methanol (CH_3OH), Guaranteed reagent grade >99.8%(GC), was purchased from KANTO CHEMICAL CO., INC.

Polyvinylidene fluoride (PVDF) (average Mw ~534,000 by GPC, Powder) and 1-Methyl-2-pyrrolidone (NMP) (MW: 99.13) were provided by Sigma Aldrich. All chemical reagents were used without any further purification.

2.2 Liquid-Mediated Synthesis of Li-Zr-F Composite

LiZrF composite was successfully synthesized with methanol as solvent. First, highly pure starting materials LiF and ZrF_4 were weighed to the stoichiometric molar ratio of LiF:ZrF_4 2:1 and dissolved in methanol media under an ambient environment, compared with water media. The suspensions were sonicated for 10 min at room temperature (RT) in air. The reaction continuously proceeded until the entire solution was completely dissolved to form a transparent solution. Subsequently, the homogeneous transparent solutions were dried at 25°C, 50°C, and 70°C in the air until all the solvent evaporated to obtain a dry precursor powder. Eventually, the precursor powders were subjected to the vacuum oven and heated at 150°C for 2 h. Finally, the LiZrF sample was subjected to the furnace for heat treatment at 200°C for 1 h to remove all impurities of organic solvent and humidity. After that the LiZrF composites were obtained. Figure 1 illustrates the various steps in preparing LiZrF composite via methanol-mediated precursor. Besides, to further evaluate the effect of vacancy concentration on the ionic conduction, LiZrF, named Li-Rich LiZrF, was synthesized via the stoichiometric molar ratio of LiF:ZrF_4 2:0.8 in methanol media and 10 min sonication at RT which was dried at 50°C/150°C under vacuum. The Li-Rich LiZrF product also was subjected to a furnace oven for post-treatment at 200°C.

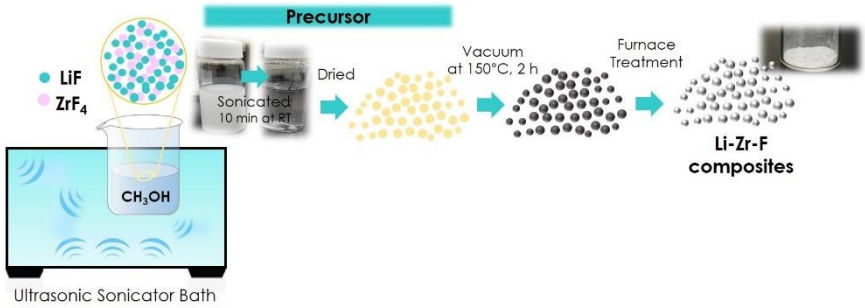

Figure 1 Schematic diagram of LiZrF composite preparation process via methanol-mediated synthesis.

2.3 Structure Characterizations

Fourier transform infrared (FTIR) spectroscopy of the precursor powder was conducted by Thermo Fisher Scientific iS50 instrument with attenuated total reflectance (ATR) iD7). The experiments were performed FT-IR in the range of 600-4000 cm^{-1} with a resolution of 4 cm^{-1} and a total of 64 scans for each sample. The crystalline structures of Li-Zr-F composites were identified by X-ray diffractometry (XRD) using a Rigaku SmartLab (Rigaku) machine equipped with Cu Kα irradiation (λ = 1.54056 Å) at an angular incidence of 10-90° (2θ angle range) with a scan speed of 2°/min and a scan step of 0.02°. The diffractogram peaks were examined using the JCPDS database. The reference intensity ratio (RIR) method, a semi-quantitative phase analysis via the X-ray powder diffraction internal standard method, was utilized to reveal the composition of the LiZrF composite, which was equivalent to the crystal phase formation obtained from XRD analysis. The influence of vacancy concentration and activation energy of ion migration was described by following the Arrhenius equation on ionic conductivity. The Boltzmann-Einstein equation was also used to describe the influence of other factors on ionic conductivity (σ) of Li-Rich LiZrF-based SE compared with LiZrF- and LiF-based SEs. Finally, the element mapping and micromorphology of LiZrF

composites were conducted by field-emission scanning electron microscopy (FESEM) with energy dispersive X-ray spectroscopy (EDX) on a JSM 7610F machine (JEOL).

2.4 Ion Conduction Performance Evaluation

The ionic conduction of Li_2ZrF_6 ($P\overline{3}1m$) composites-based SSE was examined by electrochemical impedance spectroscope (EIS) under a small amplitude alternating current (AC) potential wave with different frequencies applied to the electrochemical system. 200 mg of dried sample was cold-pressed into a polyether ether ketone (PEEK) mold with an inner diameter of 10 mm. The pellet was sandwiched between two cylindrical stainless-steel current collectors with 10 mm of diameter and pressed at a pressure of 20 MPa. The EIS measurement was carried out at the frequency range of 1 Hz-7 MHz using an electrochemical workstation in Biotech.

Later, EIS measurement was conducted on the ion-blocking symmetric batteries to calculate the temperature dependence of Li_2ZrF_6 ($P\overline{3}1m$) composites-based SSE at a temperature from 308 to 368 K (frequency ranged of 1 MHz to 0.1 Hz). Furthermore, the electronic conductivity of all samples was measured by direct current polarization tests with externally applied voltages of 0.1, 0.2, 0.3, 0.4, and 0.5 V for 1 h to reach a steady voltage.

3. Results and Discussion

A liquid-mediated precursor synthesized Li-Zr-F (LiZrF) composite under methanol (CH_3OH) solution operated under low temperature and short consuming reaction time. As shown in Figure 1, LiF and ZrF_4, as the reactance, were dispersed in CH_3OH to form the homogeneous solution under sonification at RT. Under the method-mediated synthesis, Li^+, and Zr^{4+} were combined with and F^- to trigger the precipitation of LiZrF product in the solution. The chemical structure of LiZrF composite and possible chemical structures in the methanol-mediated precursor was detected by FT-IR spectroscopy, as shown in Figure 2. The different characteristic peaks at the corresponding wavenumber could verify the specific fragment structure of organic materials in the precursor. Figure 2a shows the spectrum of LiZrF composite before heat treatment that exhibited the typical band patterns of chemical functional groups in the CH_3OH structure. The characteristic broad absorption bands around 3360 and 2900 cm^{-1} were assigned to the stretching of the -OH groups. The characteristic peak at 2921 cm^{-1} was attributed to methyl groups' symmetric C-H stretching vibrations of [28]. The strong peak at 1641 cm^{-1} and the peak at 1460 cm^{-1} corresponded to the impurity of the solvent and water vapor phase due to the presence of the deformation pattern of the OH group. The peaks frequency at 1377, 1117, and 1082 cm^{-1} were attributed to the strong stretching pattern of the C-O-H fragment related to the deformed methyl group and the absorptions at 1020 and 968 cm^{-1} corresponded to the C-H rocking vibration of methanol [10, 29]. In contrast, these absorptions disappeared in the spectrum peak of LiZrF after heat treatment, as shown in Figure 2b. The decreased intensity in the LiZrF indicated the impurity and organic fragments as the CH_3OH and humidity were completely removed by thermal treatment. As a result, it was confirmed that in the presence of a methanol-mediated precursor synergistically with heat treatment, LiF would react with ZrF_4 to establish the crystal formation of LiZrF without impurity contamination.

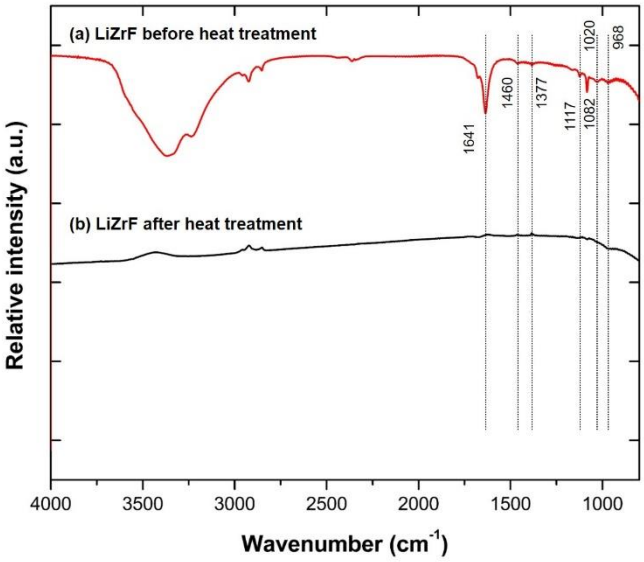

Figure 2 FTIR spectra of LiZrF (a) before and (b) after heat treatment.

The analysis of the crystal phase formation and components of LiZrF products synthesized via different mediator conditions has been conducted utilizing XRD analysis. As the consideration under the XRD database with the inorganic crystal structure database (ICSD) for compounds containing three elements, the LiZrF product was mainly three kinds of compounds including Li_2ZrF_6 with space group of $P\overline{3}1m$ (PDF#72-1291) or $P21/c$ (PDF#28-0611), and Li_4ZrF_8 with a space group of $Pnma$ (PDF#50-1317) [30]. Furthermore, to calculate the composition of LiZrF compared with LiF, the RIR equation was typically used to investigate the stoichiometric composition of material based on crystal phase from the XRD pattern [31, 32], revealed in Figure 3. Table 1 reveals the phase composition of LiZrF composites, compared among different precursors including none-mediated, H_2O-mediated, and CH_3OH-mediated precursors. Considerably, under the none-mediated pathway, the XRD pattern showed the peak of the crystal phase of reactants. It could be suggested that the reaction could not be completed within 12 hours under none-mediated synthesis leading to occurring the crystal phase of LiF and ZrF_4, as can be seen in Figure 3a. On the other hand, in underwater and CH_3OH liquid-mediated synthesis, the phase compositions of LiZrF products were significantly changed from the none mediator condition. This result implied that the mediators might improve the productive synthesis of the reaction by enhancing the reaction rate and providing the opportunity and sensitivity for the colliding of Li^+, Zr^{4+} and F^- during the propagation of the reaction. Considering water-mediated synthesis (Figure 3b), the generated LiZrF had the existence of all three-formed structures. Based on the phase diagram of the LiF-ZrF_4 system [33], the presence of such a three-phase sample was unusual because the region does not exist in the phase diagram. This phenomenon might be due to the high solubility of LiF and ZrF_4 in water, which precipitated too fast in the evaporation process of the mediator, causing the formation of a non-equilibrium phase composition.

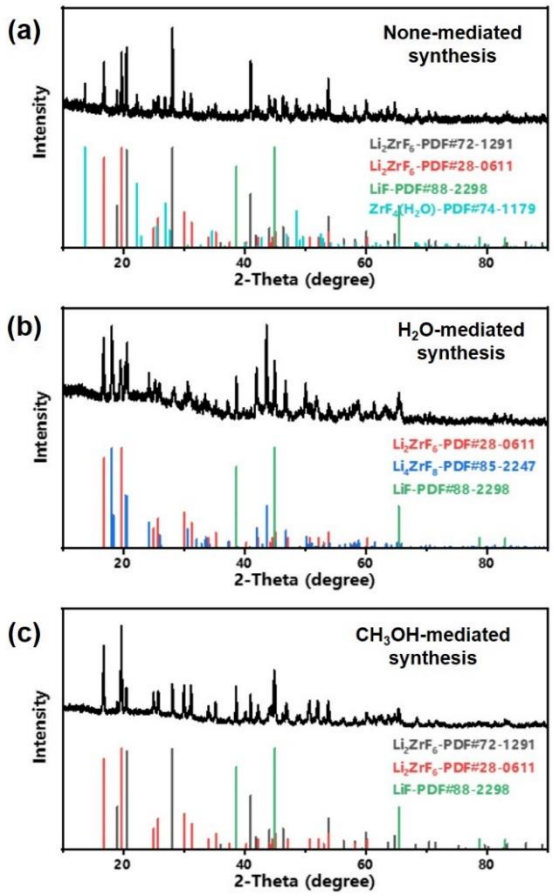

Figure 3 XRD pattern of (a) non-solvent, (b) H_2O-mediated synthesis, and (c) CH_3OH-mediated synthesis.

Table 1 Mass percentage of product phase composition of LiZrF products synthesized under different reaction conditions.

Mediator	Temperature	Product Phase Composition (wt%)		
		Li_2ZrF_6 ($P\bar{3}1m$)	Li_2ZrF_6 ($P21/c$)	Li_4ZrF_8 ($Pnma$)
None	70°C/150°C	47.2	49.7	3.1
H_2O	70°C/150°C	11.1	31.4	57.5
CH_3OH	70°C/150°C	4.4	77.1	18.5
CH_3OH	50°C/150°C	92.6	4.1	3.3
CH_3OH	25°C/150°C	N/A	N/A	N/A

On the other hand, both LiF and ZrF_4 were well dispersed under methanol solution at RT, resulting in the propagation of a non-equilibrium reaction that enhanced the composition of the LiZrF product. As shown in Figure 3c, under the methanol mediator, the XRD pattern of LiZrF exhibited the main structure of Li_2ZrF_6 ($P21/c$) phase formation with a small amount of Li_2ZrF_6 ($P\bar{3}1m$) formation. Generally, Li_2ZrF_6 ($P\bar{3}1m$) corresponded to the composition in the phase diagram at X(ZrF_4) equal to 0.33, which was preferred as the suitable crystal orientation for lithium-ion conductors [11, 19]. However, it could be noted that a part of LiF still existed in the sample, which would be caused by

the rapid precipitation rate of a small amount of LiF dissolved in methanol near the completion of the drying process. Due to the high drying rates, an unbalanced phase composition might form, resulting in an unstable thermodynamic structure and limiting the synthesized material under the temperature range operation.

To demonstrate the effect of the annealing evaporation rate of the methanol mediator on the crystal phase composition, the dried temperature condition to synthesize LiZrF was investigated under 70°C/150°C, 50°C/150°C, and 25°C/150°C. The respective XRD pattern and the phase composition analysis are shown in Figure 4 and Table 1, respectively. Figure 4a exhibits the crystal phase compositions of the LiZrF dried under the temperature condition of CH_3OH-70°C/150°C, the LiZrF composite was formed in a ternary mixture dominated by Li_2ZrF_6 ($P21/c$). Compared to the phase composition of LiZrF generated under CH_3OH-50°C/150°C (Figure 4b), the phase composition was significantly improved, which completely formed the crystal phase of Li_2ZrF_6 ($P\overline{3}1m$) without obviously impurity phase formation. This result could be suggested that the composition of the product might be effectively regulated by controlling the evaporation temperature of the mediator, and the lower evaporation rate was conducive to the formation of the equilibrium phase, which could not only improve the purity of the product, but also improve the stability of the material. Nevertheless, the reaction was difficult to occur without the external input of extra energy under the dried condition of 25°C/150°C (Figure 4c). Despite the same reaction time, almost no reactant was obtained compared to the sample obtained at 50°C/150°C. Due to many residual reactants, the composition mass fraction of dried condition at 25°C/150°C was uncounted in CH_3OH-mediated precursor. However, the reaction rate was still significantly higher than the none- mediator precursor. Hence, the experiment result suggested that the dried temperature condition of CH_3OH-50°C/150°C was considered to be the optimal reaction condition for synthesizing Li_2ZrF_6 ($P\overline{3}1m$)-SE via methanol mediated synthesis pathway. Additionally, according to the correspondence to ICSD No. PDF#72-1291, Figure 4d exhibits the crystallographic model of Li_2ZrF_6 ($P\overline{3}1m$), fluorine atoms were placed in the space with hexagonal close-packed (HCP) arrangement, this kind of arrangement is very common in structures consisting of small anions and large cations [30]. LiF_6 and ZrF_6 octahedrons are connected with a common vertex. Therefore, the chemical formula of Li_2ZrF_6 would be proposed in terms of $Li_2ZrV'_3F_6$, where V'' represented the intrinsic vacancies. These intrinsic vacancies might be essential in the ionic conductivity of the material [19].

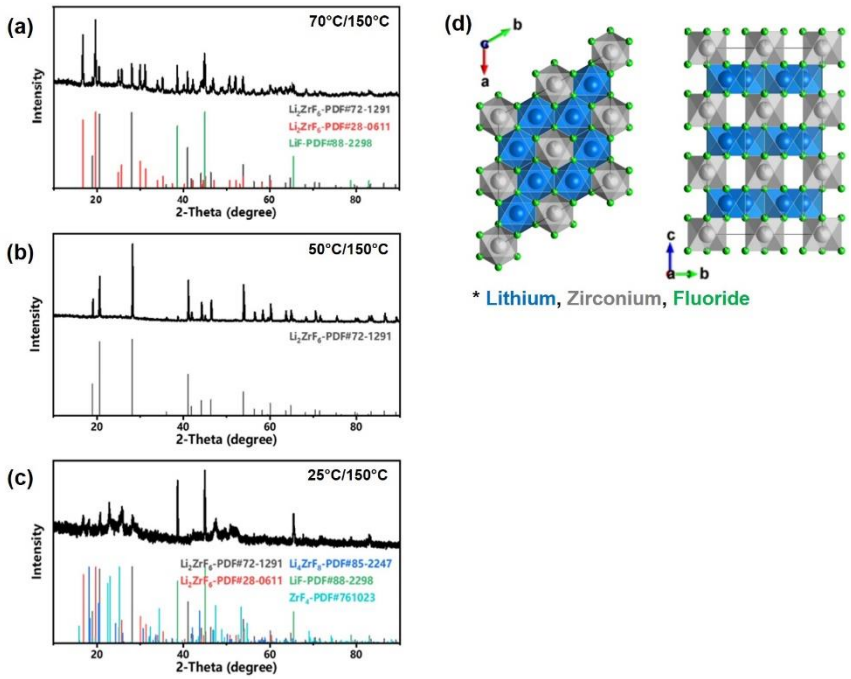

Figure 4 XRD pattern of (a) CH_3OH-70°C/150°C, (b) CH_3OH-50°C/150°C, (c) CH_3OH-25°C/150°C, and (d) crystallographic structure model of L_2ZrF_6 ($P\overline{3}1m$).

To investigate the morphology of Li_2ZrF_6 as a SE compared with LiF, FESEM analysis was indicated, as shown in Figure 5. The surface morphology of LiF (Figures 5a, b) exhibited the cubic formation of a face-centered cubic (FCC) lattice stabilized by a strong bonding between Li^+ and F^- ions. Thus, making LiF has the widest electrochemical window [18]. Although, the strong bonding between Li^+ and F^- on the one hand contributes to the high stability of LiF, it restricts the kinetic transportation of Li^+ [18, 19, 34]. Through Zr substitution via methanol-mediated synthesis, the surface morphology of the Li_2ZrF_6-based SE changed significantly with Zr^{4+} doping generating a disorder rock-salt LiF structure, as shown in Figures 5c, d. In particular, three Li^+ cations would be removed by one metal ion doping, and two vacancies would be introduced in the octahedral interstitial locations. As a result, the vacancies occupy approximately 33.3% of octahedral substitutional sites in the structure of Li_2ZrF_6. Presumably, these vacancies originated from aliovalent metal-cation doping of Li^+ and were crucial to increase the ionic conduction of Li_2ZrF_6. The grouping of vacancies and vacancy clusters within the grain boundary, crystal lattice, and defect chemistry served as important parameters for Li^+ migration via the vacancy-rich environments, which were attributed to the morphology change that significantly corresponded to the XRD pattern. Surface morphologies at different magnifications of the cathode in SSB compared between LiF and LiZrF were presented in Figures 5e, g, respectively. According to metal cation substitution in LiZrF ionic crystals with different radius atom, crystal phase might be arranged based on their electrostatic forces. As can be seen those three components in the composite cathode pellet with Li_2ZrF_6 remained in relatively closer contact than LiF without the obvious cracks in the pellet even at ultrahigh magnification. This result implied that the effective 3-dimension conduction channels for ions and electrons diffusion.

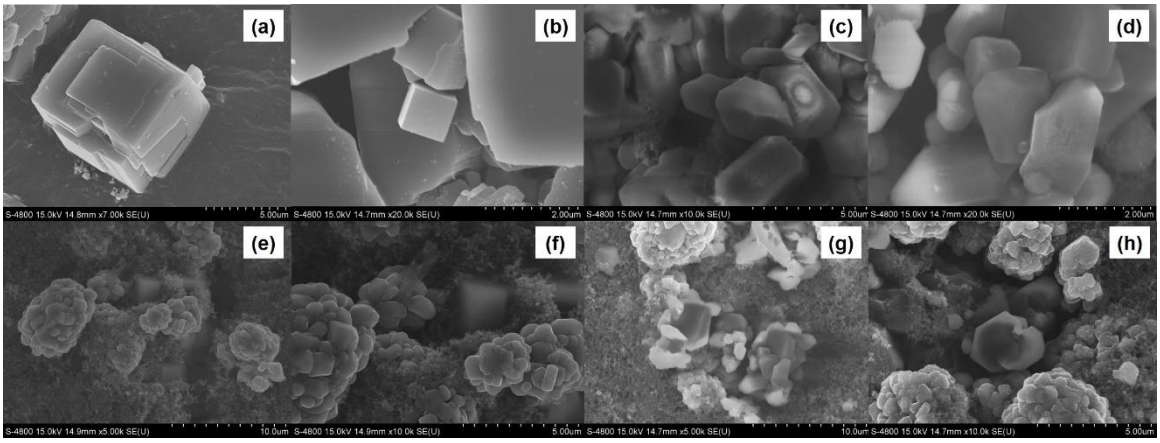

Figure 5 Surface morphology of (a,b) LiF particles, (c-d) Li_2ZrF_6 composite, composite cathode with (e-f) LiF, and (g-h) Li_2ZrF_6, respectively, at different magnifications.

Principally, EIS measurement is used to evaluate the ion conduction of the electrolyte. It is operated by applying a small amplitude AC potential wave with a different frequency to the electrochemical system and then measuring the curve of the ratio of the AC potential to the current signal with the sine wave frequency. The real part of the impedance is equal to 0 for the perfect capacitor, and then the Nyquist plot is a straight-line recombining with the imaginary axis. The ionic conductivity was calculated according to Eq. (1): [16]

$$\sigma = \frac{L}{(R\ x\ S)} \tag{1}$$

where σ is an ion conductivity (S/cm), R is the resistance determined from impedance spectra (Ω cm), L is sample thickness, and S is the contact area between two electrodes (cm^2).

The activation energy of the ion migration in the material might also be obtained according to the Arrhenius equation in Eq. (2): [16]

$$\sigma = \frac{A}{T} e^{-\frac{E_a}{k_B T}} \tag{2}$$

where σ is ionic conductivity of material, A is the Arrhenius constant, E_a is the activation energy of ion migration, k_B is the Boltzmann constant, and T is the Kelvin temperature. Then convert Eq. (2) into antiderivatives:

$$ln\sigma T = -\frac{E_a}{k_B} \cdot \frac{1}{T} + lnA \tag{3}$$

According to Eq. (3), $ln\sigma T$ is linear with $1/T$ and the slope is equal to $-E_a/k_B$. Therefore, the activation energy of ion migration can be calculated from the slope of the line obtained by plotting $ln\sigma T$ against $1/T$. It is a formulation of the relationship between temperature dependence and reaction rates. With the Arrhenius equation, it could be approximately that the ion moving rate of reaction increases with the increase of temperature leading to the enhancement of ion conductivity. The term of $e^{-E_a/k_B T}$ indicates the fraction of molecules with energy greater than or equal to E_a.

The ionic conductivity of the Li_2ZrF_6 was studied by electrochemical impedance spectroscopy (EIS). Because of an appealing feature of solid-state structures, through Zr substitution Li_2ZrF_6 by defeat chemistry could indicate the effectiveness of Li^+ hopping in the lattice. The Li^+ hopping process was sensitive to activated Li^+ and vacancy concentrations, so it could enhance conductivity by changing orders of magnitude [15] (Figure 6).

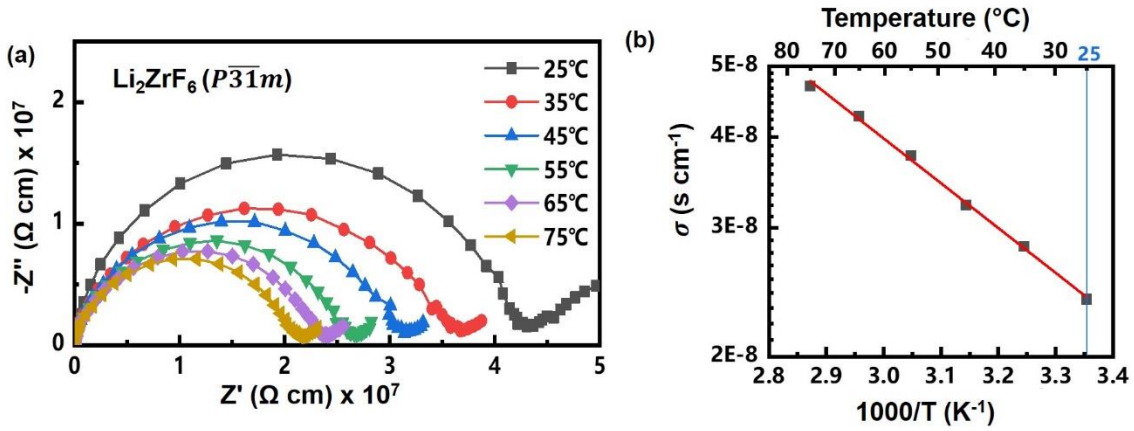

Figure 6 (a) Nyquist plots at different temperatures and (b) Arrhenius conductivity plot of Li_2ZrF_6.

The SSB system's resistance is mainly composed of three parts: bulk resistance, grain boundary resistance and electrode/electrolyte interface resistance. The equivalent circuits of these three parts can be regarded as a resistor and a capacitor in parallel, and connected in series. The resistance of each part may be different according to the material's properties, but the capacitance order is similar. The theoretical value of bulk capacitance, grain boundary capacitance and electrode/electrolyte interface capacitances are 10^{-12} F, 10^{-9} F and 10^{-6} F, and the resistance of each part can be designated. In general, the ionic conductivity of SSE is defined as the reciprocal of the sum of bulk resistance and grain boundary resistance [35, 36]. The optimally crystallized Li_2ZrF_6 synthesized under moderate conditions with a CH_3OH-mediated precursor exhibited the highest conductivity of 2.40×10^{-8} S/cm at RT with E_a evaluated at 0.15 eV. (Figure 6b). The substitution of Zr^{4+} in the optimized crystal structure of Li_2ZrF_6 ($P\overline{3}1m$) could induce the vacancies clusters. At the same time, the lattice structure would be affected by the radius of different metal cations in the metal halide electrolyte. The stacking crystal structure of metal- ion by a smaller radius Zr^{4+} ion was encouraged by an hcp-T to hcp-O transition leading to the reduction of E_a in Li_2ZrF_6 composite-based SE, compared with E_a of LiF which is equal to 0.73 eV [37]. It could be implied that the ion conduction value of Li_2ZrF_6 based SE was significantly related to the preferred orientation and the (131) plane/(001) plane peak intensity ratio in XRD patterns generated via methanol-mediated precursor.

The Li_2ZrF_6 composite material exhibited excellent defect density compared with bivalent and trivalent metal elements due to the introduction of a tetravalent element of Zr. Moreover, to demonstrate the effect of Li^+ concentration on the ion-conduction, the Li_2ZrF_6 ($P\overline{3}1m$) was synthesized from the different stoichiometric molar ratio of LiF:ZrF_4 of 2:0.8, named as Li-Rich LiZrF, which was studied and compared with LiZrF. XRD analysis demonstrated that the LiZrF and Li-Rich LiZrF products were stabilized structure by the formation of Li_2ZrF_6 ($P\overline{3}1m$).

The XRD result of the two samples was further refined with the Rietveld refinement method, a simple method widely used to demonstrate the space group, atomic coordinates and cell size [38]. The results are shown in Figure 7, Table 2 and Table 3. Due to the low atomic scattering factor of Li and F, the site occupancy information could not be accurately obtained, so the occupancy rate of Li and F had not been refined in this part. Comparing the initial reactants amount and site occupancy, the occupancy of the Zr site was different, with the decreasing molar ratio of ZrF_4, the occupancy of Zr sites decreased. The Zr content in the Li-Rich LiZrF structure was nearly 20% lower than that in LiZrF. Since the introduction of each tervalent Zr atom in Li_2ZrF_6 ($P\bar{3}1m$) would replace the surrounding four Li^+, 36.23% of the octahedral vacancy is occupied by Li^+ in LiZrF, while 39.68% was occupied by Li^+ in Li Rich-LiZrF, increasing the content of Li^+ by about 10%. Therefore, the strategy of regulating the structural characteristics by controlling the molar ratio of reactants was successed, the number of vacancies in the material could be adjusted effectively, and the concentration of lithium ions in the material was significantly increased.

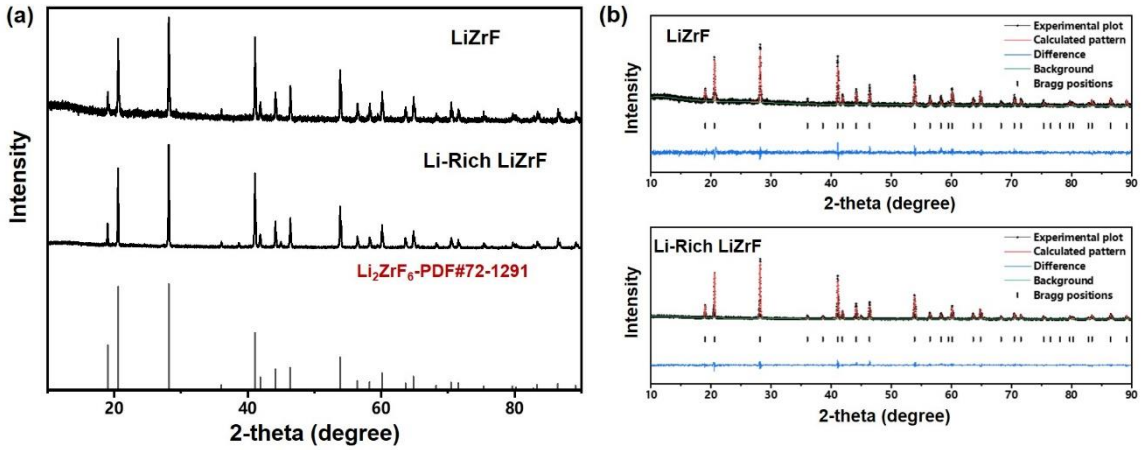

Figure 7 (a) XRD pattern and (b) the corresponding Rietveld refinements of LirZF compared with Li-Rich LiZrF, respectively.

Table 2 Refined parameters and crystallographic data of LiZF and Li-Rich LiZF.

Sample	**LiZrF**	**Li-Rich LiZrF**
Radiation	Cu kα	
2θ interval (°)	10-90	
Rwp (%)	15.510	15.847
Space group	P-31 m	
a = b (Å)	4.97418	4.97383
c (Å)	4.65695	4.65628
α = β (°)	90	
γ (°)	120	
V (Å^3)	99.787	99.759

Table 3 Rietveld refinement results of LiZrF and Li-Rich LiZrF.

Sample	Atom	x	y	z	Occ.	Sym.
LiZrF	Li	0.33330	0.66670	0.50000	1.0000	m
	Zr	0.00000	0.00000	0.00000	0.8785	32
	F	0.34000	0.00000	0.26131	1.0000	-3 m
Li-Rich LiZrF	Li	0.33330	0.66670	0.50000	1.0000	m
	Zr	0.00000	0.00000	0.00000	0.7550	32
	F	0.33797	0.00000	0.26089	1.0000	-3 m

EIS also studied the ion conduction of Li-Rich LiZrF compared to LiZrF. The Li-Rich LiZrF and LiZrF pellets were sandwiched between two cylindrical stainless-steel current collector measurements. From the electrochemical impedance data, the diameter of the semicircle is characteristic of the bulk interfacial resistance of electrolytes between electrodes. Following Eq. (1) and (2), Figure 8a shows the respective ionic conductivity of Li-Rich LiZrF with the reciprocal of temperature. The ionic conductivity of Li-Rich LiZrF at room temperature was nearly twice increased to 3.89×10^{-8} S/cm with E_a of 0.21 eV (Figure 8b) while the LiZrF exhibited only 2.40×10^{-8} S/cm which were considered by the Boltzmann-Einstein equation [39, 40]. Following the relation between these equations, it could be implied that the addition of the sited-number of ions per unit volume (vacancy, Z) by increasing the Li^+concertation led to enhancement of the available ion movement. The electronic conductivity of the material was also measured by DC polarization under applying constant potential. Due to a blocking electrode, the electrode cannot provide ions, which are polarized at the electrode. After the ions in the material were exhausted, it was difficult for the ions to continue moving, so the movement of electrons only generated the current at this time. The electrical conductivity can be evaluated by using Eq. (4):

$$\sigma = \left[\frac{\Delta V}{I} \times \frac{w \cdot t}{s}\right]^{-1} \quad (4)$$

where σ is an electron conductivity (S/cm), ΔV is voltage is difference, I is the applied current, w is the diameter of SE pellet, t is the SE pellet thickness, and s is the electrode separation.

The test results are shown in Figure 8c, d, and the calculated electronic conductivity of Li-Rich LiZrF was 3.42×10^{-9} S/cm, which was lower than the ionic conduction of Li-Rich LiZrF, approximately 10% of the overall conductivity [41]. The addition of functional lithium-fluoride contents could appear to be a facile synthesis with the simple method to suppress Li dendrites by reducing the compact conformal SEI layer [42]. In addition, Li-Rich LiZrF also proposed the from these experiment results, it could be expected that Li-Rich LiZrF was employed as an alternative material for solid electrolyte promising for the future development of all-solid-state lithium batteries.

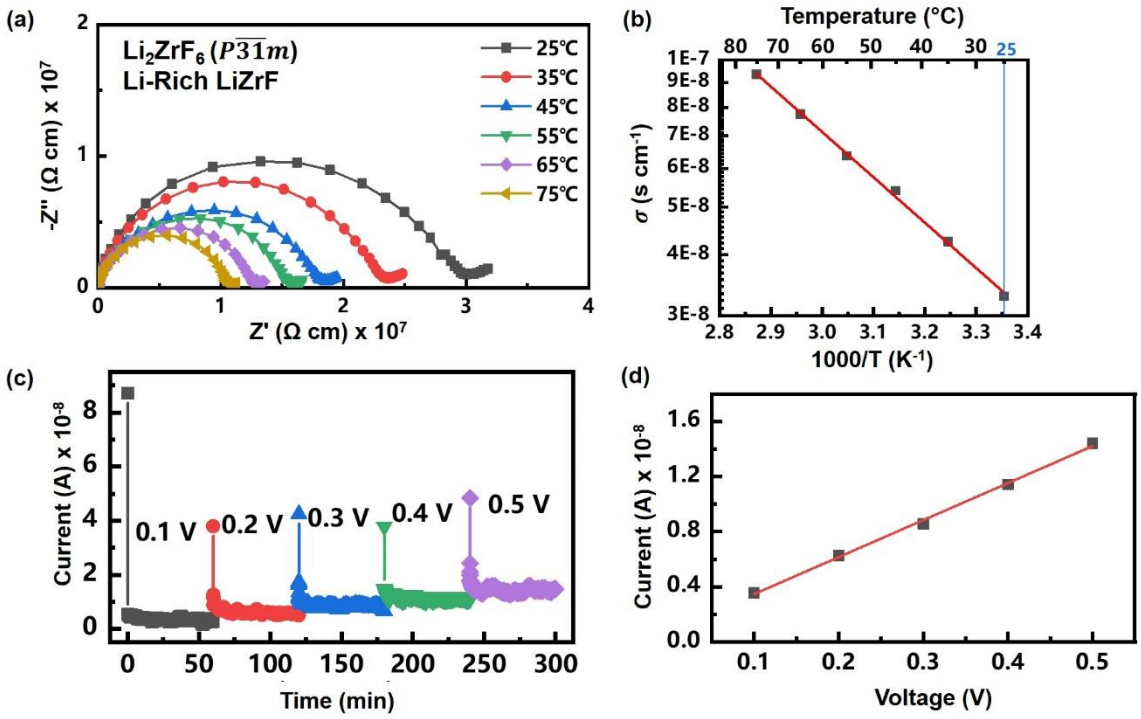

Figure 8 (a) Nyquist plots at different temperatures, (b) Arrhenius conductivity plot, (c) DC polarization curves, and (d) equilibrium current response at different voltages of Li-Rich LiZrF, respectively.

4. Conclusion

In this work, a novel method route with methanol precursor has been proposed for synthesizing LiZrF electrolytes. Li_2ZrF_6 was successfully synthesized by a simple one-step method, and the effects of different mediators, the stoichiometric molar ratio of LiF:ZrF_4 and temperature conditions on the synthesis were discussed. The annealing dried condition of CH_3OH-50°C/150°C was considered the optimal reaction condition for synthesizing Li_2ZrF_6 ($P\bar{3}1m$)-SE via methanol mediated synthesis pathway. Moreover, the ionic conduction of the material was further improved by adjusting the proportion of the initial reactants generated in terms of Li-Rich LiZrF Li_2ZrF_6 ($P\bar{3}1m$)-SE. The obtained ionic conduction was increased to 3.89×10^{-8} S/cm, and the E_a of ion migration was equal to 0.21 eV. The lower E_a of Li_2ZrF_6 than the LiF through the substitution of Zr^{4+} would be suggested that the framework of LiZrF-based SE was formed by the sublattice stacked layer of anion and influenced by the volume and polarity of the cation species leading to enhancement of ion conduction, which was demonstrated outstanding electrochemical performance. Besides, the substitution of Zr^{4+} in the crystallographic layer also affected the air stabilization of LiZrF-based SE electrolytes greater than sulfide-based SEs. Experimental results suggested that our development of the synthesized LiZrF-based SE via a methanol-mediated precursor provided a simple method at mild conditions that could improve the ion conductivity of LiF.

Acknowledgments

The authors are grateful for the financial support of this research from Japan Science and Technology Agency, Strategic International Collaborative Research Program (Grant No.:

JPMJSC18H1) and Japan Science and Technology Agency, Open Innovation Platform with Enterprises, Research Institute and Academia (Grant No.: JPMJOP1843).

Author Contributions

The manuscript was written through the contributions of all authors. All authors have given approval to the final version of the manuscript. Conceptualization: N. Saito; Methodology: J. Moon and R. Zheng; Investigation (experimental work): J. Moon, R. Zheng, and S. Liu; Writing original draft: J. Moon, R. Zheng, and S. Thiangtham; Writing review and editing: S. Thiangtham and C. Chokradjaroen; Supervision: N. Saito; Funding acquisition: N. Saito and Y. Sawada.

Competing Interests

The authors declare no competing financial interest.

References

1. Thongwichit N, Li OL, Yaowarat W, Saito N, Suriyapraphadilok U. Adsorption of carbon dioxide by solution-plasma-synthesized heteroatom-doped carbon nanospheres. Jpn J Appl Phys. 2015; 55: 01AE10.
2. Huo H, Gao J, Zhao N, Zhang D, Holmes NG, Li X, et al. A flexible electron-blocking interfacial shield for dendrite-free solid lithium metal batteries. Nat Commun. 2021; 12: 176.
3. Zhang Y, Huang J, Saito N, Yang X, Zhang Z, Yang L, et al. Layered perovskite lithium yttrium titanate as a low-potential and ultrahigh-rate anode for lithium-ion batteries. Adv Energy Mater. 2022; 12: 2200922.
4. Liao F, Molin E, van Wee B. Consumer preferences for electric vehicles: A literature review. Transp Rev. 2017; 37: 252-275.
5. Zhu F, Islam MS, Zhou L, Gu Z, Liu T, Wang X, et al. Single-atom-layer traps in a solid electrolyte for lithium batteries. Nat Commun. 2020; 11: 1828.
6. Lin D, Liu Y, Cui Y. Reviving the lithium metal anode for high-energy batteries. Nat Nanotechnol. 2017; 12: 194-206.
7. Yang Q, Li C. Li metal batteries and solid state batteries benefiting from halogen-based strategies. Energy Stor Mater. 2018; 14: 100-117.
8. Liu J, Bao Z, Cui Y, Dufek EJ, Goodenough JB, Khalifah P, et al. Pathways for practical high-energy long-cycling lithium metal batteries. Nat Energy. 2019; 4: 180-186.
9. Yin YC, Wang Q, Yang JT, Li F, Zhang G, Jiang CH, et al. Metal chloride perovskite thin film based interfacial layer for shielding lithium metal from liquid electrolyte. Nat Commun. 2020; 11: 1761.
10. Luo X, Cai D, Wang X, Xia X, Gu C, Tu J. A novel ethanol-mediated synthesis of superionic halide electrolytes for high-voltage all-solid-state lithium–metal batteries. ACS Appl Mater Interfaces. 2022; 14: 29844-29855.
11. Luo X, Wu X, Xiang J, Cai D, Li M, Wang X, et al. Heterovalent cation substitution to enhance the ionic conductivity of halide electrolytes. ACS Appl Mater Interfaces. 2021; 13: 47610-47618.
12. Li X, Liang J, Chen N, Luo J, Adair KR, Wang C, et al. Water-mediated synthesis of a superionic halide solid electrolyte. Angew Chem. 2019; 131: 16579-16584.

13. Gao Z, Sun H, Fu L, Ye F, Zhang Y, Luo W, et al. Promises, challenges, and recent progress of inorganic solid-state electrolytes for all-solid-state lithium batteries. Adv Mater. 2018; 30: 1705702.
14. Ren Y, Qi Z, Zhang C, Yang S, Ma X, Liu X, et al. The charge transfer of intercalated Li atoms around islands on Li-halide (F, Br, Cl) surface of SEIs: A first principles calculation. Comput Mater Sci. 2020; 176: 109535.
15. Asano T, Sakai A, Ouchi S, Sakaida M, Miyazaki A, Hasegawa S. Solid halide electrolytes with high lithium-ion conductivity for application in 4 V class bulk-type all-solid-state batteries. Adv Mater. 2018; 30: 1803075.
16. Xie J, Sendek AD, Cubuk ED, Zhang X, Lu Z, Gong Y, et al. Atomic layer deposition of stable $LiAlF_4$ lithium ion conductive interfacial layer for stable cathode cycling. Acs Nano. 2017; 11: 7019-7027.
17. Oi T. Ionic conductivity of LiF thin films containing Di-or trivalent metal fluorides. Mater Res Bull. 1984; 19: 451-457.
18. Zhang B, Zhong J, Zhang Y, Yang L, Yang J, Li S, et al. Discovering a new class of fluoride solid-electrolyte materials via screening the structural property of Li-ion sublattice. Nano Energy. 2021; 79: 105407.
19. Liang J, Li X, Adair KR, Sun X. Metal halide superionic conductors for all-solid-state batteries. Acc Chem Res. 2021; 54: 1023-1033.
20. Bachman JC, Muy S, Grimaud A, Chang HH, Pour N, Lux SF, et al. Inorganic solid-state electrolytes for lithium batteries: Mechanisms and properties governing ion conduction. Chem Rev. 2016; 116: 140-162.
21. Lieser G, Winkler V, Geßwein H, de Biasi L, Glatthaar S, Hoffmann MJ, et al. Electrochemical characterization of monoclinic and orthorhombic Li_3CrF_6 as positive electrodes in lithium-ion batteries synthesized by a sol–gel process with environmentally benign chemicals. J Power Sources. 2015; 294: 444-451.
22. Fan S, Lei M, Wu H, Hu J, Yin C, Liang T, et al. A Na-rich fluorinated sulfate anti-perovskite with dual doping as solid electrolyte for Na metal solid state batteries. Energy Stor Mater. 2020; 31: 87-94.
23. Van der Ven A, Bhattacharya J, Belak AA. Understanding Li diffusion in Li-intercalation compounds. Acc Chem Res. 2013; 46: 1216-1225.
24. Feinauer M, Euchner H, Fichtner M, Reddy MA. Unlocking the potential of fluoride-based solid electrolytes for solid-state lithium batteries. ACS Appl Energy Mater. 2019; 2: 7196-7203.
25. Huang H, Wu HH, Chi C, Yang Y, Zheng J, Huang B, et al. Phase-structure-dependent Na ion transport in yttrium-iodide sodium superionic conductor Na_3YI_6. J Mater Chem. 2021; 9: 26256-26265.
26. Li C, Gu L, Maier J. Enhancement of the Li conductivity in LiF by introducing glass/crystal interfaces. Adv Funct Mater. 2012; 22: 1145-1149.
27. Hu J, Yao Z, Chen K, Li C. High-conductivity open framework fluorinated electrolyte bonded by solidified ionic liquid wires for solid-state Li metal batteries. Energy Stor Mater. 2020; 28: 37-46.
28. Thiangtham S, Runt J, Manuspiya H. Sulfonation of dialdehyde cellulose extracted from sugarcane bagasse for synergistically enhanced water solubility. Carbohydr Polym. 2019; 208: 314-322.

29. Eck M. Performance enhancement of hybrid nanocrystal-polymer bulk heterojunction solar cells: Aspects of device efficiency, reproducibility, and stability. Breisgau: Albert-Ludwigs-Universität Freiburg; 2014.
30. Li X, Liang J, Yang X, Adair KR, Wang C, Zhao F, et al. Progress and perspectives on halide lithium conductors for all-solid-state lithium batteries. Energy Environ Sci. 2020; 13: 1429-1461.
31. Hubbard CR, Snyder RL. RIR-measurement and use in quantitative XRD. Powder Diffr. 1988; 3: 74-77.
32. Schreiner WN. A standard test method for the determination of RIR values by x-ray diffraction. Powder Diffr. 1995; 10: 25-33.
33. Beneš O, Konings RJM. Thermodynamic study of LiF–BeF_2–ZrF_4–UF_4 system. J Alloys Compd. 2008; 452: 110-115.
34. Sheng O, Jin C, Ding X, Liu T, Wan Y, Liu Y, et al. A decade of progress on solid-state electrolytes for secondary batteries: Advances and contributions. Adv Funct Mater. 2021; 31: 2100891.
35. Li X, Liang JW, Chen N, Luo J, Adair KR, Wang C, et al. Water-mediated synthesis of a superionic halide solid electrolyte. Angew Chem Int Ed. 2019; 58: 16427-16432.
36. Zhang D, Nakano H, Yamamoto K, Tanaka K, Yahara T, Imai K, et al. Rate-determining process at electrode/electrolyte interfaces for all-solid-state fluoride-ion batteries. ACS Appl Mater Interfaces. 2021; 13: 30198-30204.
37. Tan J, Matz J, Dong P, Shen J, Ye M. A growing appreciation for the role of LiF in the solid electrolyte interphase. Adv Energy Mater. 2021; 11: 2100046.
38. Rietveld HM. A profile refinement method for nuclear and magnetic structures. J Appl Crystallogr. 1969; 2: 65-71.
39. Tomita Y, Fuji-i A, Ohki H, Yamada K, Okuda T. New lithium ion conductor Li_3InBr_6 studied by ^7Li NMR. Chem Lett. 1998; 27: 223-224.
40. Tomita Y, Yonekura H, Yamauchi Y, Yamada K, Kobayashi K. Substitution effect in the ion conductor Li_3InBr_6, studied by nuclear magnetic resonance. Z Naturforsch A. 2002; 57: 447-450.
41. Gao D, Zeng Z, Mi H, Sun L, Ren X, Zhang P, et al. Enhanced structural stability and overall conductivity of Li-rich layered oxide materials achieved by a dual electron/lithium-conducting coating strategy for high-performance lithium-ion batteries. J Mater Chem A. 2019; 7: 23964-23972.
42. Hu J, Chen K, Li C. Nanostructured Li-rich fluoride coated by Ionic liquid as high ion-conductivity solid electrolyte additive to suppress dendrite growth at Li metal anode. ACS Appl Mater Interfaces. 2018; 10: 34322-34331.